Analysis and Linearization of a Broadband Microwave Phase Modulator Using Volterra System Approach

Patrick Celka, *Member, IEEE,* Martin J. Hasler, *Fellow, IEEE,* and Ataollah Azizi

***Abstract*— In this paper, a Volterra system approach is employed to analyze a nonlinear delay line that is used as a broadband phase modulator. Computed response waveform of the modulator in the time domain is compared with experimental results in order to confirm the Volterra system approach. The phase versus voltage characteristics of the modulator is then linearized using a predistortion circuit in which the parameters are derived from the Volterra kernels. Harmonic and intermodulation distortions are calculated with and without the predistortion circuit. It is shown that the use of the predistortion circuit results in a considerable reduction of these distortions.**

I. Introduction

BROADBAND PHASE modulators have numerous applications in both microwaves and telecommunications [1]–[4]. For the transmission of analog signals, the linearity of the modulator becomes the primary concern. The phase modulator studied in this paper is a nonlinear delay line. It consists of a high-impedance transmission line, periodically loaded by a number of reverse-biased hyperabrupt varactor diodes at regular time intervals τ. The varactor diodes act as variable shunt capacitances, providing a variable delay of a signal propagating on the line as a function of the applied voltage.

Such nonlinear transmission lines are used to generate electrical pulses with rise times in the order of few picoseconds [5]–[8] and can also be employed as a broadband phase modulator. Superimposing on the line a carrier with a modulating signal and a proper dc bias results in phase modulation [5]. Due to the nonlinear nature of the C-V curve of a varactor diode, the phase versus voltage characteristics of the delay line are also nonlinear. For small variations of the voltage on the line, the nonlinearity is relatively mild and the Volterra series can be used to study the dynamic characteristics of the phase modulator.

After the characterization of the phase nonlinearity, a predistortion circuit is proposed to reduce the second and third order harmonics (HD_2, HD_3) and intermodulation (IMD_{20}, IMD_{21}) distortion produced by the modulator.

The paper is organized as follows. The second part of the paper is mainly devoted to describe the phase modulator as well as the model and parameters representing the varactor diodes. In the third part, Volterra kernels are computed up to the third order and the time response of the modulator of a sine wave input is computed and compared with experimental results. The fourth part of the paper describes the predistortion circuit and results of the Volterra system model, showing the improvement in the overall linearity and the reduction of IMD_{20} and IMD_{21}.

Manuscript received March 8, 1996; revised March 26, 1996.

P. Celka is with the Department of Electrical Engineering, Signal Processing Laboratory, Swiss Federal Institute of Technology, CH-1015 Lausanne, Switzerland.

M. J. Hasler is with the Department of Electrical Engineering, Chaire des Circuits et Systèmes, Swiss Federal Institute of Technology, 1015 Lausanne, Switzerland.

A. Azizi is with Ascom-Tech Ltd., Corporate Research Division, 3018 Bern, Switzerland.

Publisher Item Identifier S 0018-9480(96)08507-9.

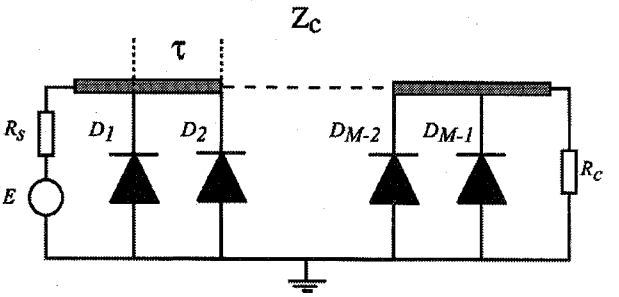

Fig. 1. Circuit diagram of the TWPM.

II. The Phase Modulator

The structure of the phase modulator is depicted in Fig. 1. A high-impedance (Z_c) transmission line is loaded by $M-1$ reverse-biased GaAs hyperabrupt varactor diodes at regular time intervals τ. The structure is referred to as the travelling wave phase modulator (TWPM). By properly choosing the parameters of the TWPM (Z_c, τ, M), relatively low insertion loss and small input and output VSWR is obtained. In the experimental modulator, 50 varactor diodes were used to load a 90-Ω microstrip transmission line at regular time intervals of 30 ps on a teflon substrate. A 10-dB chip attenuator is used at the output for reducing eventual reflections. It should also be pointed out that in the experimental phase modulator, statistical dispersion in the capacitance versus voltage characteristics of the 50 diodes were relatively important.

The TWPM can be considered as a cascade of $M-1$ basic units (cells), each one consisting of a piece of transmission line T_i (whose length is defined by τ), shunted by the varactor

0018–9480/96$05.00 © 1996 IEEE

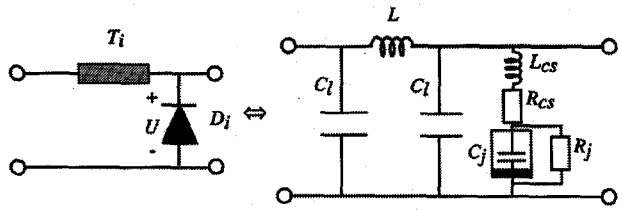

Fig. 2. Equivalent circuit of a piece of transmission line shunted by a varactor diode.

TABLE I
PARAMETER VALUES

$R_s[\Omega]$	$R_L[\Omega]$	$L[nH]$	$C_l[pF]$	R_{cs} $[\Omega]$
50	50	2.7	0.3	1.5

L_{cs} $[nH]$	R_j $[M\Omega]$	$\Phi[V]$	γ	$C_0[pF]$
0.45	1	1.3	2	10.5

diodes D_i. Fig. 2 shows the equivalent circuit of one of these basic units.

The capacitance and inductance of the piece T_i are C_l and L, respectively. The overall cutoff frequency of the line is given by: $f_c \approx 1/\pi\sqrt{L(C_j + C_l)}$. The cutoff frequency of the TWPM is about 4.9 GHz with parameter of Table I. The model parameters of the hyperabrupt varactors of Fig. 2 are defined as [9]:

R_{cs} substrate and bond resistance;
L_{cs} series inductance;
R_j p-n junction resistance;
C_j junction capacitance;
C_0 projected zero bias voltage capacitance;
γ junction doping profile exponent;
Φ junction built in potential.

Within a limited interval, the junction capacitance C_j of a varactor diode as a function of the applied reverse voltage U can be approximated by

$$C_j(U) = \frac{C_0}{(1 + U/\Phi)^\gamma}. \tag{1}$$

In Fig. 3, relation (1) represents the straight line. For hyperabrupt GaAs junctions, the exponent γ is approximately 2 and the junction built in potential $\Phi = 1.3$.

The curve of Fig. 3 shows an average capacitance versus bias voltage V_r^0 for 50 packaged varactor diodes. It should be pointed out that the measured C-V characteristics of 50 varactor diodes presented significant dispersion in some regions (>50 %), but for the Volterra series analysis the averaged curve of Fig. 3 and the relation (1) are used. Relation (1) is valid for values of V_r^0 between 2.7 and 4.7 V (Fig. 3). Table I summarizes the values of the parameters that are used for the Volterra system model of TWPM.

These values are obtained through a series of measurements (dc and S-parameter) on a number of varactor diodes. Preliminary studies based on the calculation of the scattering parameters of the whole structure (TWPM) have permitted the optimization of the parameters of the transmission line Z_c and τ and the number of varactors $M - 1$ to insure low input and output VSWR. It appears that the actual value of series resistors R_{cs} is higher than the value taken from the calculations, which is responsible for the slightly higher insertion loss in the experimental results. The complete model of the TWPM is illustrated in Fig. 4.

The input signal $e(t)$ is composed of a carrier signal S_c, a modulating signal S_m, and a dc bias voltage V_r^0. Due to the ladder structure of the circuit, recurrence relations between the currents and voltages at different nodes can be established and the Volterra kernels for the output voltage can be calculated.

III. THE VOLTERRA SYSTEM APPROACH

We will show that the Volterra system theory [10] is a powerful tool and can be used to analyze the behavior of the circuit, characterize its nonlinearities, and calculate the intermodulation products. The Volterra series expansion of one variable of the circuit has normally an infinite number of terms. Depending on the nature of the nonlinearity and the accuracy of the approximation we want to reach, a limited number of terms can be used, and we thus get a polynomial system. In the present case we truncated after the third term giving rise to a third-order polynomial system. This approximation will be justified by the good correspondence between the model and the measurements done. Each term of the truncated serie is characterized by its kernel, which in turn can be defined either in the time or Laplace domain. We use the Laplace domain representation and define the three kernels related to the output voltage $U_{\text{out}}(p)$ by: $H_{\text{out}}^{(n)} = H_M^{(n)}, n = 1, \cdots, 3$. Once we have computed these kernels, temporal responses and output phase characteristic of the TWPM will be evaluated. In order to give some hints about the Volterra kernels computation, we introduce the following notation according to the circuit of Fig. 4: $H_k^{(n)}(p_1, \cdots, p_n)$ is the nth-order kernels of the kth cell voltage $U_k, G_k^{(n)}(p_1, \cdots, p_n)$ the nth-order kernel of I_k and $J_k^{(n)}(p_1, \cdots, p_n)$ the nth order-kernel of the charge Q_k in the kth nonlinear capacitance C_j. The charge is given by $Q_k(U_k) = C_j(U_k)U_k \equiv h(U_k)$. A third-order Taylor expansion of the function $h(U)$ around V_r^0 is given by $h(U) \approx \Sigma_{n=1}^3 a_n(V_r^0)\ \Delta U^n$ with $U = V_r^0 + \Delta U$, where $a_n(V_r^0)$ represents the coefficient of the nth term of the polynomial approximation of $h(U)$. These coefficients vary as a function of the bias and so do the Volterra kernels[1]. From $h(U)$, we can compute the following relations between $J_k^{(n)}(p_1, \cdots, p_n)$ and $H_k^{(n)}(p_1, \cdots, p_n)$:

$$\begin{aligned}
J_k^{(1)} &= a_1 H_k^{(1)}(p_1) \\
J_k^{(2)} &= a_1 H_k^{(2)}(p_1, p_2) + a_2 H_k^{(1)}(p_1) H_k^{(1)}(p_2) \\
J_k^{(3)} &= a_1 H_k^{(3)}(p_1, p_2, p_3) + a_2 (H_k^{(1)}(p_1) H_k^{(2)}(p_2, p_3) \\
&\quad + H_k^{(1)}(p_3) H_k^{(2)}(p_1, p_2)) \\
&\quad + a_3 H_k^{(1)}(p_1) H_k^{(1)}(p_2) H_k^{(1)}(p_3).
\end{aligned} \tag{2}$$

[1]Explicit dependence in $H_{\text{out}}^{(n)} = H_M^{(n)}$ expressions on V_r^0 will be avoided in later sections.

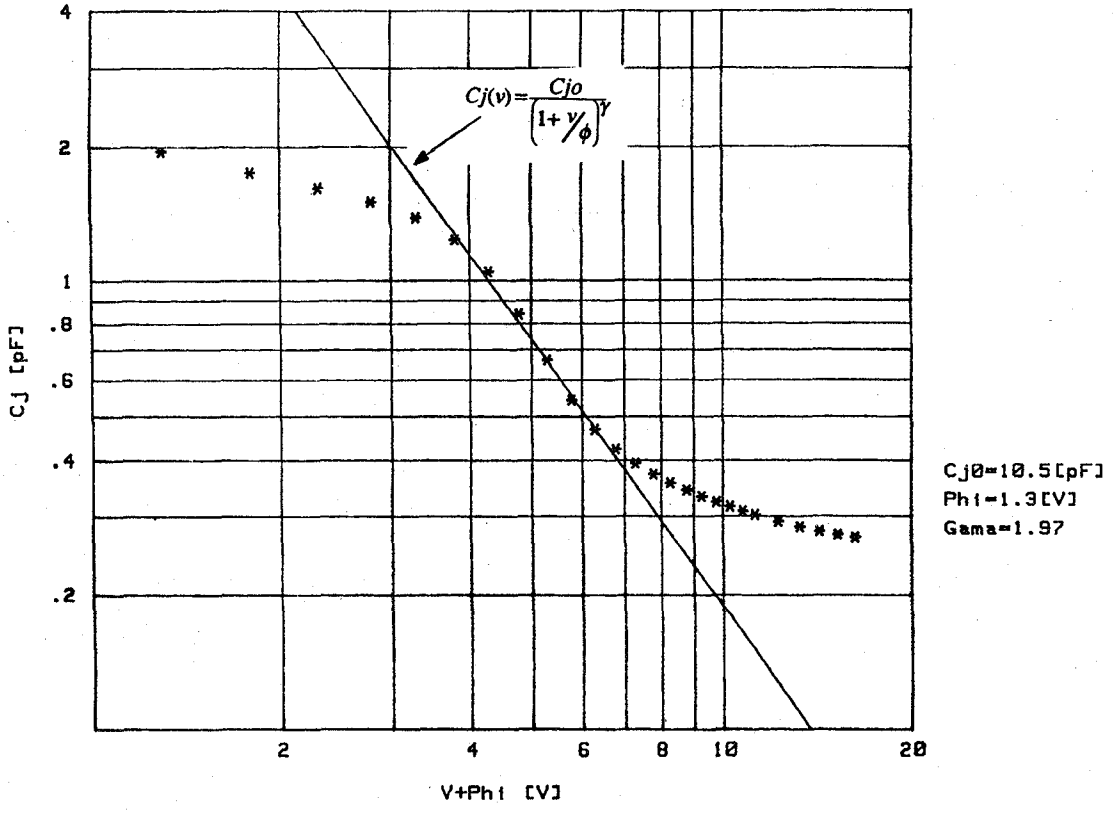

Fig. 3. Typical capacitance variation of a hyperabrupt varactor diode as a function of the applied reverse voltage V_r^0.

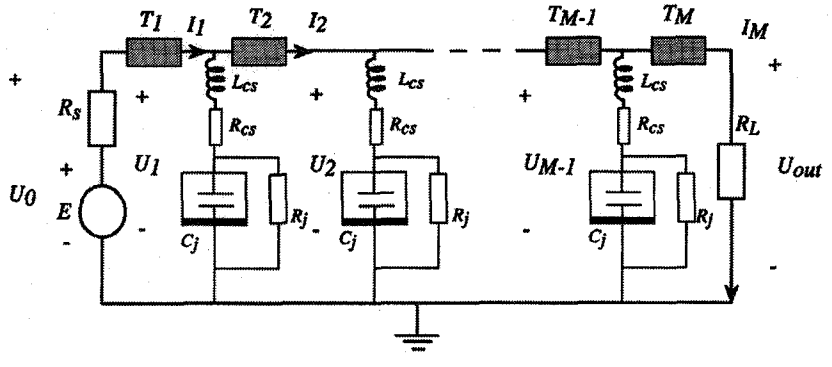

Fig. 4. The model TWPM.

The voltage applied to one diode is U and the current is $I_D = I_{DC_j} + I_{DR_j}$ where I_{DC_j} is the current across the capacitance C_j and I_{DR_j} is the current across the resistance R_j; thus, we have $U = U_j + (R_{cs} + L_{cs}p)\,(U_j + R_j p \Sigma_{i=1}^{3}\, a_i\, U_j^i)/R_j$ where U_j is the voltage applied to C_j only. Neglecting the current across the resistor R_j, we can define the impedance of the linearized diode as $Z_D = U/I_{DC_j}$. Finally the impedance $Z_D[p] = (R_{cs} + L_{cs}p) + R_j/(1 + pa_1R_j)$ in parallel with the two impedance C_l will be called Z_{DT}. Due to the ladder topology of the circuit, we can establish the following reccurence relations between[2] $G_{k+1}^{(n)}$ and $H_k^{(n)}$.

[2]The square bracket $[p]$ refer to Laplace argument p in impedances like quantities.

With $p_{\Sigma(n)} = \Sigma_{k=1}^{n}\, p_k$ we get the following reccurence relations:

$$H_k^{(n)}(p_1, \cdots, p_n) = H_{k-1}^{(n)}(p_1, \cdots, p_n) - G_k^{(n)}(p_1, \cdots, p_n) Z_T[p_{\Sigma(n)}] \quad (3)$$

$$G_{k+1}^{(n)}(p_1, \cdots, p_n) = G_k^{(n)}(p_1, \cdots, p_n) - J_k^{(n)}(p_1, \cdots, p_n) p_{\Sigma(n)}. \quad (4)$$

with $Z_T[p] = Lp$. In (4), the term $a_1 p$ represents the inverse of the impedance of the linearized diode and must be replaced by $1/Z_D[p]$ as we have mentioned above. These relations will be useful in the computation of the second- and third-order kernels. Let us define the following matrices in order to

simplify the notation for the kernels:

$$T_i[p] \equiv \begin{bmatrix} 1 & Z_T[p_{\Sigma(i)}] \\ 1/Z_{DT}[p_{\Sigma(i)}] & 1+Z_T[p_{\Sigma(i)}]/Z_{DT}[p_{\Sigma(i)}] \end{bmatrix} \tag{5}$$

$$\begin{aligned} A_{11}^k[p] &\equiv T_1^k(1,1) + T_1^k(1,2)/R_L \\ A_{12}^k[p] &\equiv T_1^k(2,1) + T_1^k(2,2)/R_L \\ A_{21}^k[p_1,p_2] &\equiv T_2^k(1,1) + T_2^k(1,2)/R_L \\ A_{22}^k[p_1,p_2] &\equiv T_2^k(2,1) + T_2^k(2,2)/R_L \\ A_{31}^k[p_1,p_2,p_3] &\equiv T_3^k(1,1) + T_3^k(1,2)/R_L \\ A_{32}^k[p_1,p_2,p_3] &\equiv T_3^k(2,1) + T_3^k(2,2)/R_L. \end{aligned} \tag{6}$$

We are now ready to compute the Volterra kernels $H_M^{(n)}$. The first order kernel is simply the impulse response of the linearized circuit and is given by $H_M^{(1)} = H_{\text{out}}^{(1)} = U_M/E$ where E is the input signal in the Laplace domain. The relation between the vector $(U_1\ I_1)^T$ and $(U_M\ I_M)^T$ is

$$\begin{pmatrix} U_1 \\ I_1 \end{pmatrix} = T_1^{M-1} \begin{pmatrix} U_M \\ I_M \end{pmatrix} \tag{7}$$

and the boundary conditions on the circuit are

$$U_0 = U_1 + I_1 Z_T \tag{8}$$

$$E = U_0 + R_S I_1 \tag{9}$$

$$U_M = R_L I_M \tag{10}$$

and thus with (7)–(10) we get

$$H_{\text{out}}^{(1)} = (A_{11}^{M-1}[p] + (Z_T[p] + R_S)A_{12}^{M-1}[p])^{-1}. \tag{11}$$

The second-order kernel is computed with (2)–(4) and we obtain

$$\begin{aligned} &\begin{pmatrix} H_k^{(2)} \\ G_k^{(2)} \end{pmatrix} \\ &= T_2^{M-k}[p_1,p_2] \begin{pmatrix} H_M^{(2)} \\ G_M^{(2)} \end{pmatrix} \\ &\quad + \sum_{n=1}^{M-k-1} T_2^n[p_1,p_2] \\ &\quad \times \begin{pmatrix} 0 \\ a_2 p_{\Sigma(2)} A_{11}^{M-k-n}[p_1] A_{11}^{M-k-n}[p_2] H_M^{(1)}(p_1) H_M^{(1)}(p_2) \end{pmatrix} \\ &\quad + \begin{pmatrix} 0 \\ a_2 p_{\Sigma(2)} H_k^{(1)}(p_1) H_k^{(1)}(p_2) \end{pmatrix}. \end{aligned} \tag{12}$$

The boundary conditions on the second-order kernels are $H_0^{(2)} = -R_S G_1^{(2)}, H_0^{(2)} = H_1^{(2)} + G_1^{(2)} Z_T[p_{\Sigma(2)}]$ and $H_M^{(2)} = R_L G_M^{(2)}$, so we get the relation between $G_1^{(2)}$ and $H_1^{(2)}$: $H_1^{(2)} = -(R_S + Z_T[p_{\Sigma(2)}])G_1^{(2)}$. This last expression with (12), computed for $k = 1$, gives the result for the second-order kernel

$$\begin{aligned} &H_M^{(2)}(p_1,p_2) \\ &\quad = -\left\{ \frac{(R_S + Z_T[p_{\Sigma(2)}])P_{1G} + P_{1H}}{A_{21}^{M-1}[p_1,p_2] + (R_S + Z_T[p_{\Sigma(2)}])A_{22}^{M-1}[p_1,p_2]} \right\} \\ &\qquad \times H_M^{(1)}(p_1) H_M^{(1)}(p_2) \end{aligned} \tag{13}$$

with the polynomials P_{1G} and P_{1H} given by

$$P_{1H} = \sum_{k=1}^{M-2} T_2^k(1,2) a_2 p_{\Sigma(2)} A_{11}^{M-k-1}[p_1] A_{11}^{M-k-1}[p_2] \tag{14}$$

$$\begin{aligned} P_{1G} = &\sum_{k=1}^{M-2} T_2^k(2,2) a_2 p_{\Sigma(2)} A_{11}^{M-k-1}[p_1] A_{11}^{M-k-1}[p_2] \\ &+ a_2(p_{\Sigma(2)}) A_{11}^{M-1}[p_1] A_{11}^{M-1}[p_1]. \end{aligned} \tag{15}$$

To calculate the third-order kernel, the same procedure as for the second-order gives the final result, shown in (16) at the bottom of the page, with the polynomials P_{2G} and P_{2H} given by

$$P_{2G} = \sum_{n=1}^{M-2} T_3^n(2,2)(V2_{n+1} + V3_{n+1}) + V2_1 + V3_1 \tag{17}$$

$$P_{2H} = \sum_{n=1}^{M-2} T_3^n(1,2)(V2_{n+1} + V3_{n+1}). \tag{18}$$

If we introduce the notation $H_M^{(2)}(p_1,p_2) \equiv B[p_1,p_2] H_M^{(1)}(p_1) H_M^{(1)}(p_2)$, we have the relations (19), (20) for polynomials $V2_k[p_1,p_2,p_3]$ and $V3_k[p_1,p_2,p_3]$

$$V3_k = a_3 p_{\Sigma(3)} A_{11}^{M-k}[p_1] A_{11}^{M-k}[p_2] A_{11}^{M-k}[p_3] \tag{19}$$

$$\begin{aligned} V2_k = a_2 p_{\Sigma(3)} \{ &A_{11}^{M-k}[p_1](A_{21}^{M-k}[p_2,p_3] B[p_2,p_3] \\ &+ P_{1H}^{(k)}[p_2,p_3] + P_{1G}^{(k)}[p_2,p_3]) \\ &+ A_{11}^{M-k}[p_3](A_{21}^{M-k}[p_1,p_2] B[p_1,p_2] \\ &+ P_{1H}^{(k)}[p_1,p_2] + P_{1G}^{(k)}[p_1,p_2])\}. \end{aligned} \tag{20}$$

The polynomials P_{2G}, P_{2H}, P_{1G}, and P_{1G} in p_k are functions of the parameters of Table I and of the coefficients $a_n(V_r^0), n = 1, \cdots, 3$. The output voltage in the time domain $u_{\text{out}}(t)$ is the sum of three terms depending on the Volterra kernels $h_{\text{out}}^{(n)}(t_1, \cdots, t_n) = \mathcal{L}^{-1}[H_{\text{out}}^{(n)}(p_1, \cdots, p_n)]$ and the input signal $e(t)$: $u_{\text{out}}(t) \approx u_1(t) + u_2(t) + u_3(t)$ where

$$\begin{aligned} u_n(t) = &\int_{-\infty}^{+\infty} h_{\text{out}}^{(n)}(\sigma_1, \cdots, \sigma_n) e(t-\sigma_1) \\ &\cdots e(t-\sigma_n)\, d\sigma_1 \cdots\, d\sigma_n \end{aligned} \tag{21}$$

for $n = 1,2,3$. In order to compute the nth-order time response $u_n(t)$, we have to evaluate one inverse multiple Laplace transform $\mathcal{L}^{-1}$ of the kernel $H_{\text{out}}^{(n)}(p_1, \cdots, p_n)$ and

$$H_M^{(3)}(p_1,p_2) = -\left\{ \frac{(R_S + Z_T[p_{\Sigma(3)}])P_{2G} + P_{2H}}{A_{31}^{M-1}[p_1,p_2,p_3] + (R_S + Z_T[p_{\Sigma(3)}])A_{32}^{M-1}[p_1,p_2,p_3]} \right\} \times H_M^{(1)}(p_1) H_M^{(1)}(p_2) H_M^{(1)}(p_3) \tag{16}$$

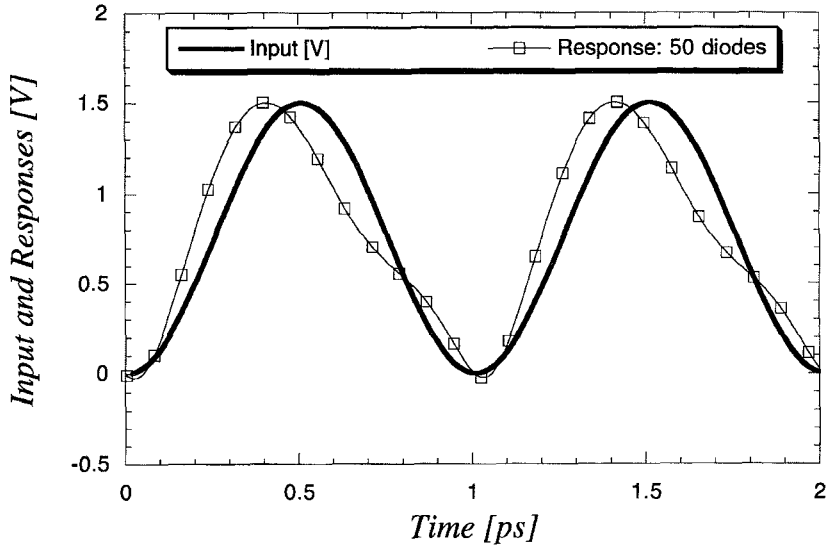

Fig. 5. Calculated results showing the formation of shock waves in TWPM ($f_0 = 1$ GHz). The bold line is the input and the square marked line is the output signal.

n integrals. We can simplify this by using the so-called associated transform [10, Theorem 2.7]. The Laplace transform of the output voltage can be written by the sum of the following three terms:

$$U_{\text{out}}(p) = U_1(p) + U_2(p) + U_3(p) \tag{22}$$

where

$$U_1(p) = H_{\text{out}}^{(1)}(p)E(p) \tag{23}$$

$$U_2(p) = \int_\Gamma H_{\text{out}}^{(2)}(p_1, p-p_1)E(p_1)E(p-p_1)\,dp_1 \tag{24}$$

$$U_3(p) = \int_{\Gamma\times\Gamma} H_{\text{out}}^{(3)}(p_1, p_2-p_1, p-p_2)E(p_1) \cdot E(p_2-p_1)E(p-p_2)\,dp_1\,dp_2 \tag{25}$$

and Γ is the imaginary axis. The relations (21)–(24) will be used to calculate the response of the modulator in the time domain. They require only $n-1$ integrations for the nth-order term and one simple Laplace transform $E(p) = \mathcal{L}[e(t)]$ and inverse Laplace transform $u_{\text{out}}(t) = \mathcal{L}^{-1}[U_{\text{out}}(p)]$. The nth-order kernel is proportional to the product of n first-order kernels as it can be seen from (13) and (16). Moreover the T_i are symmetrical in p_k, so the nth-order kernel is symmetrical in p_k. This property allows us to reduce the computation complexity.

IV. Time Domain Responses

Several authors [7], [11]–[13] have studied the formation of shock waves on the nonlinear delay line of Fig. 1. To ensure that the third-order Volterra model describes the circuit behavior correctly, the time domain response of the circuit is calculated and compared with the experimental results. First relations (21)–(24) are used to compute the response in the frequency domain. The temporal response is then obtained by inverse Fourier transformation. At a dc bias of 4 V, a 1.5 V peak-peak sine wave is fed on the line. The calculated and experimental results are shown in Figs. 5 and 6, respectively.

Keeping in mind that the experimental results are obtained with an additional 10-dB attenuation and that the phase difference was adjusted manually to about 180° in order to clearely observed both waveforms, a closer look at Figs. 5 and 6 reveals that the calculated and measured results are in good agreement.

The compression phenomena has already been observed by Rodwell *et al.* [5], [6], [8], Freeman and Karbowiak [12], Jäger and Tegude [13] or Camacho-Peñalosa and Molina-Fernandez [14] . A comparison with results of [14], in which they use a harmonic balance analysis, and those of [13], in which they use partial differential equations, also confirms that the third-order Volterra model can correctly represent the behavior of the delay line, provided the applied signals are limited to the region where the junction capacitance of the varactor diodes can be represented by (1). The oscillations shown in the output waveforms of [14] and [13] could also be reproduced with the Volterra kernels using smaller values of R_{cs}, lower input frequencies f_0, and small values of the bias point V_r^0.

V. Phase Modulation

Here, the input signal $e(t)$ is composed of a carrier signal $S_c(t) = V_r \cos(\omega_0 t)$ and a bias voltage V_r^0. The carrier frequency f_0 is an important parameter and should be chosen far away from the cutoff frequency. As it was already mentioned, the Volterra kernels depend on the bias voltage $H_{\text{out}}^{(n)} = H_{\text{out}}^{(n)}(V_r^0)$. Phase modulation is characterized by calculating and plotting the phase φ of the output signal as a function of the bias voltage V_r^0, for a given carrier frequency. The output signal $S(\omega_0)$ in the frequency domain that can be calculated from relations (21)–(24) is given by

$$S(\omega_0) = \sum_{n=1}^{\infty} C_n(V_r^0, \omega_0) = S_0 e^{j\varphi(V_r^0, \omega_0)} \tag{26}$$

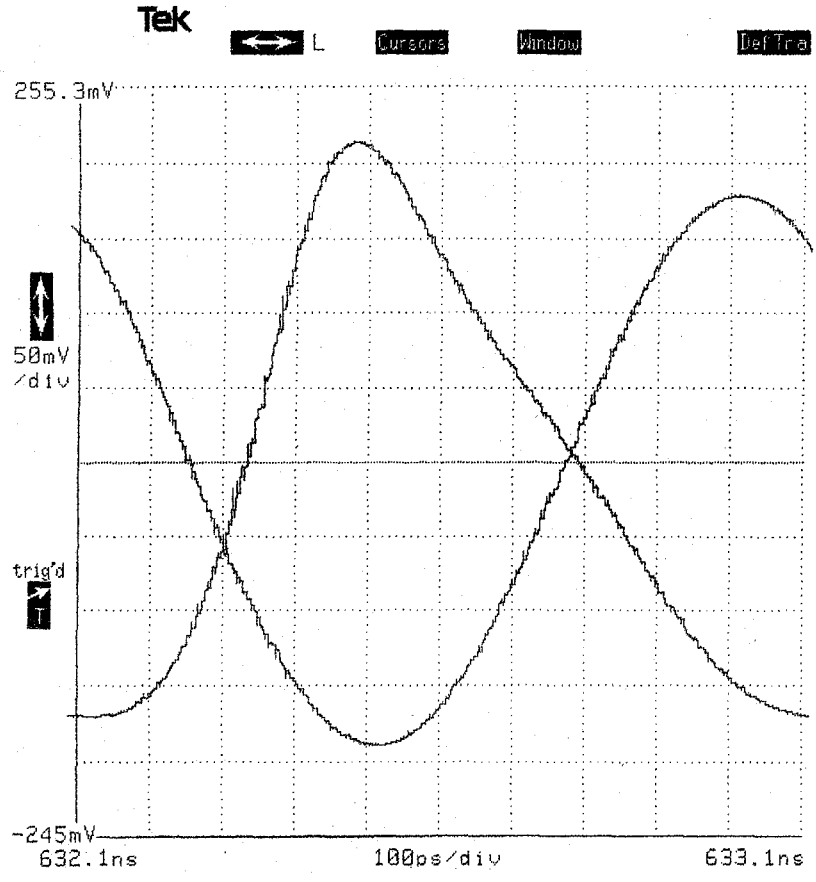

Fig. 6. Measured results showing shock wave formation in TWPM ($f_0 = 1$ GHz).

with $f_0 = \omega_0/2\pi$

$$C_n = \sum_{k=1}^{\infty} \sum_{\substack{n_1+\cdots+n_k=n \\ n_i=\pm 1}} \left(\frac{V_r}{2}\right)^k H_{\text{out}}^{(k)}(n_1 j\omega_0, \cdots, n_n j\omega_0). \tag{27}$$

With the Volterra series being limited to the third order, we obtain

$$C_1 \approx \left(\frac{V_r}{2}\right) H_{\text{out}}^{(1)}(j\omega_0) + 3\left(\frac{V_r}{2}\right)^3 H_{\text{out}}^{(3)}(j\omega_0, -j\omega_0, j\omega_0) \tag{28}$$

$$C_2 \approx \left(\frac{V_r}{2}\right)^2 H_{\text{out}}^{(2)}(j\omega_0, j\omega_0) \tag{29}$$

$$C_3 \approx \left(\frac{V_r}{2}\right)^3 H_{\text{out}}^{(3)}(j\omega_0, j\omega_0, j\omega_0) \tag{30}$$

$$C_n \approx 0 \quad \text{for} \quad n > 3. \tag{31}$$

The coefficients C_n depend on the bias voltage and the carrier frequency. Finally, the phase is obtained by

$$\varphi(V_r^0, \omega_0) = \text{Arg}[C_1(V_r^0, \omega_0) + C_2(V_r^0, \omega_0) + C_3(V_r^0, \omega_0)]. \tag{32}$$

Fig. 7 shows the normalized phase at the output of TWPM as a function of the bias voltage for three different frequencies and an input signal of 100 mV peak to peak.

It is noted that for the carrier frequencies of 1 and 2 GHz the calculated results are in close agreement with measured ones. At 3 GHz the discrepancy between the two results become more important, which is mainly due to the increase of dispersion in the experimental delay line. Same type of nonlinearity is observed in both results, which of course in a multitone phase modulation scheme will produce harmonics and intermodulation products. The next section is devoted to the study of these distortions.

VI. Harmonic and Intermodulation Distortions

Distortion produced by TWPM are high order harmonics (HD_2 and HD_3) and intermodulation products (IMD_{20} and IMD_{21}), which are studied in this section using the usual two-tone test.

A. Harmonic Distortions

Assuming a bias voltage V_r^0, the phase at the output which is defined by (16), is approximated by a Taylor series expansion around V_r^0. For a given input signal $E(t) = S_c(t) + V_r^0$, the phase can be written as

$$\varphi(V_r, V_r^0, t) = \sum_{k=0}^{\infty} \frac{\varphi^{(k)}(V_r^0, \omega_0)}{k!} V_r^k \cos^k(\omega_0 t) \tag{33}$$

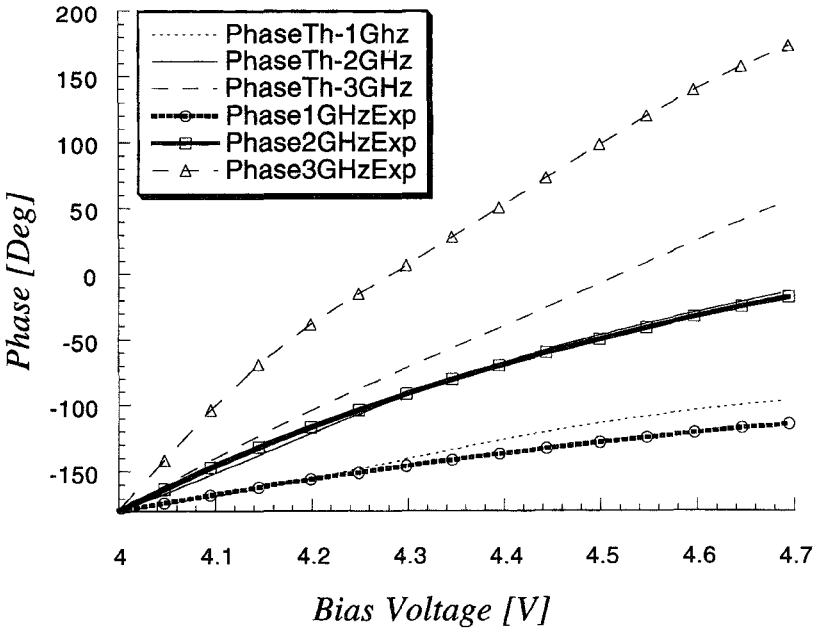

Fig. 7. The computed (thin lines) and measured (bold lines) phase φ versus the bias voltage V_r^0 for three carrier frequencies.

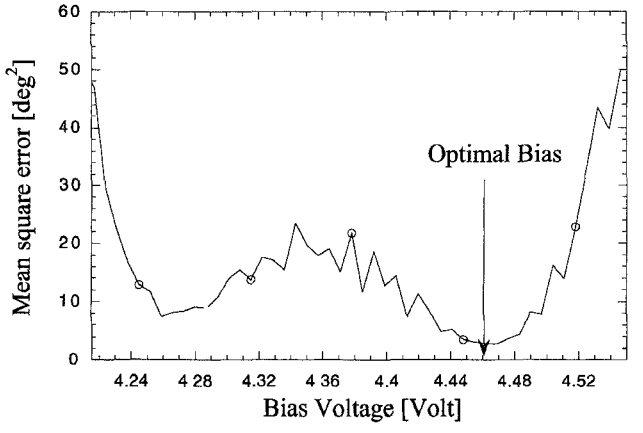

Fig. 8. The mean square error as a function of V_r^*.

or

$$\varphi(V_r, V_r^0, t) = \sum_{l=0}^{\infty} C_l \cos(l\omega_0 t) \tag{34}$$

where $\varphi^{(k)} \equiv d^k/d(V_r^0)^k$

After some algebra [see Appendix A, (A1)–(A3)] the harmonic distortion terms HD_2 and HD_3 are found, and given by the following:

$$HD_2 \approx \left| \frac{6\varphi^{(2)}(V_r^0)V_r^2}{24\varphi^{(1)}(V_r^0)V_r + 3\varphi^{(3)}(V_r^0)V_r^3} \right| \tag{35}$$

and

$$HD_3 \approx \left| \frac{\varphi^{(3)}(V_r^0)V_r^3}{24\varphi^{(1)}(V_r^0)V_r + 3\varphi^{(3)}(V_r^0)V_r^3} \right|. \tag{36}$$

Once again the coefficients $\varphi^{(k)}(V_r^0)$ depend on the Volterra kernels [see Appendix A, (A1)–(A3)].

B. Intermodulation Distortions

For calculating IMD_{20} and IMD_{21}, a two-tone test is employed [9]. The same conditions as in Section III-D are assumed with the only difference that $S_c(t)$ is composed of two signals of slightly different frequencies

$$S_c(t) = V_r(\cos(2\pi f_1 t) + \cos(2\pi f_2 t)). \tag{37}$$

The phase is now given by

$$\varphi(V_r, V_r^0, t) = \sum_{k=|m|+|l|=0}^{\infty} C_k \cos((2m\pi f_1 + 2l\pi f_2)t). \tag{38}$$

The coefficients C_k, which are calculated in Appendix B, enable us to define the IMD's. Finally

$$IMD_{20} \approx \left| \frac{2\varphi^{(3)}(V_r^0, \omega_0)V_r^2}{8\varphi^{(1)}(V_r^0, \omega_0)V_r + 3\varphi^{(3)}(V_r^0, \omega_0)V_r^3} \right| \tag{39}$$

$$IMD_{21} \approx \left| \frac{6\varphi^{(3)}(V_r^0, \omega_0)V_r^3}{8\varphi^{(1)}(V_r^0, \omega_0)V_r + 3\varphi^{(3)}(V_r^0, \omega_0)V_r^3} \right|. \tag{40}$$

VII. Predistortion Circuit

In this section we study a predistortion circuit, which when used with TWPM, will result in an improvement of the linearity and consequently in an important reduction of the distortions.

A. Design of the Predistortion Circuit

Once again, (16) is replaced by a second-order Taylor expansion $P_2(V_r^0, V_r^*)$, around a bias voltage V_r^*. It can be shown that there exists an optimal bias point where the mean square error between the calculated and approximated phase $\left\|\varphi(V_r^0) - P_2(V_r^0, V_r^*)\right\|_{L_2}$ is minimum (Fig. 8). This optimum bias is then chosen for further developments.

The following is the second-order Taylor approximation of the theoretical curve of Fig. 7 for $f_0 = 2$ GHz

$$P_2(V_r^0, V_r^*) = \varphi(V_r^*) + \varphi^{(1)}(V_r^*)(V_r^0 - V_r^*) + \frac{\varphi^{(2)}(V_r^*)}{2}(V_r^0 - V_r^*)^2 \quad (41)$$

or

$$P_2(V_r^0, V_r^*) = \alpha_0 + \alpha_1 V_r^0 + \alpha_2 (V_r^0)^2. \quad (42)$$

The optimal bias point is $V_r^* = 4.469$ V. The polynomial coefficients α_i in (23) depend on the Volterra kernels. The next step is to find a voltage transformation $V_r^0 \rightarrow \hat{V}_r^0$ ($\hat{V}_r^0$ being the distorted voltage), such that the new phase $\hat{\varphi}(\hat{V}_r^0)$ is approximately linear, i.e., $\hat{\varphi}(\hat{V}_r^0) \approx b_0 + b_1 \hat{V}_r^0$. In the bias interval $[V_{r-}^0, V_{r+}^0]$ one obtains

$$b_0 = \frac{\varphi(V_{r+}^0)V_{r-}^0 - \varphi(V_{r-}^0)V_{r+}^0}{V_{r-}^0 - V_{r+}^0} \quad (43)$$

$$b_1 = \frac{\varphi(V_{r-}^0) - \varphi(V_{r+}^0)}{V_{r-}^0 - V_{r+}^0}. \quad (44)$$

By taking $\hat{\varphi}(\hat{V}_r^0) \approx P_2(V_r^0, V_r^*)$ with V_r^* being the optimal bias, it is easy to show that the desired transformation is given by

$$\hat{V}_r^0 = V_r^0 + k(V_r^0 - V_{\min})^2 \quad (45)$$

with

$$k = \frac{\alpha_2}{b_1} \quad (46)$$

$$V_{\min} = \sqrt{\frac{\alpha_0 - b_0}{\alpha_2}}. \quad (47)$$

If we assume that the transformation in (26) is also valid for ac voltages, we can decompose the voltage V into a dc V^0 and ac V_{ac} part: $V = V^0 + V_{\text{ac}}$, and when in (26) V_r^0 is replaced by V the following is obtained:

$$\hat{V} = (V^0 + k\Delta V^2) + V_{\text{ac}}(1 + 2k\Delta V) + kV_{\text{ac}}^2 \quad (48)$$

or

$$\hat{V} = V_{\text{dc}} + A_0 V_{\text{ac}} + A_1 V_{\text{ac}}^2. \quad (49)$$

The ΔV, which is given by $\Delta V = V^0 - V_{\min}$, is determined by the maximum amplitude of a modulating signal to insure a peak phase excursion within the voltage range of 2.7–4.7 V. The modulating signal $S_m(t)$ goes first through a predistortion circuit before getting combined with the carrier signal $S_c(t)$ and fed into the modulator. The linearized phase for $f_0 = 2$ GHz, $V_r^* = 4.469$ V, $k = -0.735$ and $V_{\min} = 4.345$ V (resulting in the following predistortion coefficients: $V_{\text{dc}} = 4.578$ V, $A_0 = 0.559$ and $A_1 = -0.735$ V^{-1}) is shown in Fig. 9.

Obviously with predistortion the linearity of the modulator improves considerably. In the next section the IMD's with and without the predistortion circuit are calculated.

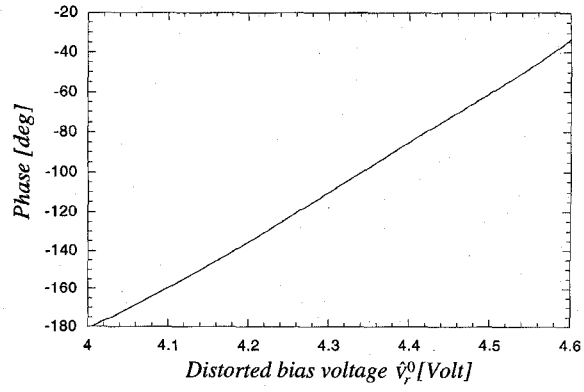

Fig. 9. The phase variation as a function of the predistorted bias voltage $\hat{V}_r^0$.

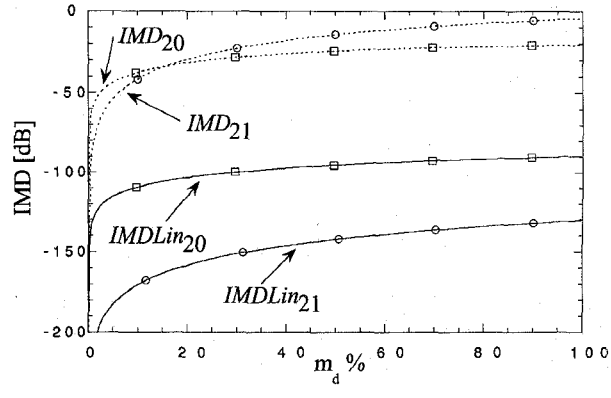

Fig. 10. Comparison of the intermodulation products $IMD_{20}(\diamond)$ and $IMD_{21}(\circ)$ between the linearized and the nonlinearized modulators.

B. Evaluation of the Linearity with the Predistortion Circuit

In this section the intermodulation products (IMD_{20} and IMD_{21}) are calculated from (21) as a function of the modulation depth m_d (with respect to $\Delta V = 300$ mV) around the optimum bias voltage. Fig. 10 shows these products for both the linearized and the nonlinearized modulators, for a carrier frequency of 2 GHz

As a consequence of improvement in the linearity of the modulator by the predistortion circuit, an important reduction in the intermodulation products is achieved. For instance for a modulation depth $m_d = 20\%$, a decrease of about 70 dB in IMD_{20} and more than 125 dB for IMD_{21} is obtained.

VIII. Conclusion

We have used the third-order Volterra series to analyze the behavior of a broadband microwave phase modulator, which is principally a nonlinear delay line. The modulator consists of a high-impedance transmission line shunted by a number of hyperabrupt varactor diodes at regular time intervals.

The structure is analyzed in both the time and frequency domains and results are in good agreement with the measurements. A method based on the Volterra kernels is used to calculate the harmonic and intermodulation distortions. After characterizing the nonlinearity of the phase versus voltage, a predistortion circuit is proposed to linearize this characteristic. A simple method is then presented to determine the parameters of the predistortion circuit. Analysis of the modulator with the

predistortion circuit reveals the improvement in the linearity and decrease of the intermodulation products.

APPENDIX A

Relations defining harmonic distortions are derived here. With the following notation $\varphi(V_r^0) \equiv \varphi(V_r^0, \omega_0)$ and $F_i \equiv \varphi^{(i)}(V_r^0)/i!$, one can find the expression for C_{2l} and C_{2l+1}

$$C_{2l} = \sum_{i=l}^{\infty} F_{2i} V_r^{2i} a_{2l}^{(2i)} \quad \text{and} \quad C_{2l+1} = \sum_{i=l}^{\infty} F_{2i+1} V_r^{2i+1} b_{2l+1}^{(2i+1)} \tag{A1}$$

where the coefficients $a_{2l}^{(n)}$ and $b_{2l+1}^{(n)}$ are given by the recurrence law

$$\begin{aligned} a_{2l}^{(2i)} &= \tfrac{1}{2}(\alpha(l) b_{2l-1}^{(2i-1)} + b_{2l+1}^{(2i-1)}) \\ b_{2l+1}^{(2i+1)} &= \tfrac{1}{2}(\alpha(l) a_{2l}^{(2i)} + a_{2l+2}^{(2i)}) \end{aligned} \quad \text{with} \quad \begin{aligned} l &= 0, \cdots, i \\ i &= 0, \cdots, \infty \end{aligned} \tag{A2}$$

and

$$\begin{aligned} \alpha(l) &= 2 \quad \text{for} \quad l = 0 \\ \alpha(l) &= 1 \quad \text{for} \quad l = 1, \cdots, i-1 \\ \alpha(l) &= 0 \quad \text{for} \quad l = i. \end{aligned} \tag{A3}$$

The initial value for the iterative calculation of (A2) is $a_0^{(0)} = 1$. The harmonic distortion of the phase associated with the frequency kf_0 is defined by the following

$$HD_k = \left| \frac{C_k}{C_1} \right| \tag{A4}$$

APPENDIX B

The expressions for IMDs that are derived here refer to Section III-D. The same notations as in Appendix A are taken here. In its most general form of the phase of the output signal in a two-tone modulation scheme is given by

$$\begin{aligned} \varphi(V_r, V_r^0, t) = &\sum_{k=0}^{\infty} F_{2k} V_r^{2k} \sum_{\substack{|m|+|l|=2i \\ i=0,\cdots,k}}^{2k} c_{|m||l|}^{(2k)} \\ &\cdot \cos((2m\pi f_1 + 2l\pi f_2)t) \\ &+ \sum_{k=0}^{\infty} F_{2k+1} V_r^{2k+1} \sum_{\substack{|m|+|l|=2i+1 \\ i=0,\cdots,k}}^{2k+1} c_{|m||l|}^{(2k+1)} \\ &\cdot \cos((2m\pi f_1 + 2l\pi f_2)t). \end{aligned} \tag{B1}$$

A more closed form of (B1) is given in (38) where the coefficients $C_k, k = |m| + |l|$, are defined as

$$C_{2n=|m|+|l|} = \sum_{k=n}^{\infty} F_{2k} V_r^{2k} \sum_{|m|+|l|=2n} c_{|m||l|}^{(2k)} \tag{B2}$$

and

$$C_{2n+1=|m|+|l|} = \sum_{k=n}^{\infty} F_{2k+1} V_r^{2k+1} \sum_{|m|+|l|=2n+1} c_{|m||l|}^{(2k+1)}. \tag{B3}$$

The following terms defining $c_{|m||l|}^{(n)}$ are used to calculate IMP_{20} and IMP_{21}: $c_{00}^{(0)} = 1$, $c_{10}^{(1)} = 1$, $c_{20}^{(2)} = 1/2$, $c_{11}^{(2)} = 1$, $c_{00}^{(2)} = 1$, $c_{30}^{(3)} = 1/4$, $c_{21}^{(3)} = 3/4$, $c_{10}^{(3)} = 9/4$. The intermodulation distortion of order (m, l) or IMD_{ml} is given by the following relation:

$$IMD_{ml} = \left| \frac{\displaystyle\sum_{\substack{k=|m|+|l| \\ k \text{ odd or even}}}^{\infty} F_k V_r^k c_{|m||l|}^{(k)}}{\displaystyle\sum_{\substack{k=1 \\ k \text{ odd}}}^{\infty} F_k V_r^k c_{10}^{(k)}} \right|. \tag{B4}$$

REFERENCES

[1] E. C. Niehenke, V. V. DiMarco, and A. Friedberg, "Linear analog hyperabrupt varactor diode phase shifters," in *IEEE MTT-S Dig.*, 1985, vol. 1, pp. 657–660.

[2] S. Lucyszyn and J. D. Robertson, "Synthesis techniques for high performance octave bandwidth 180° analog phase shifters," *IEEE Trans. Microwave Theory Tech.*, vol. 4, pp. 731, 1992.

[3] R. A. Cryan, R. T. Unwin, I. Garreit, M. J. N. Sibley, and N. M. Calcert, "Optical fiber digital pulse-position-modulation assuming a gaussian received pulse shape," *IEE Proc. J.*, vol. 137, no. 2, pp. 89–96, 1990.

[4] S. Suzuki, T. Takeuchi, K. Kaede, and B. Hirosaki, "Evolutional approach to the fiber to the home with novel analog catv distribution system," in *Proc. ISSLS*, Apr. 1991, vol. 9, pp. 425–431.

[5] M. J. W. Rodwell, D. M. Bloom, and B. A. Auld, "Nonlinear transmission line for picosecond pulse compression and broadband phase modulation," *Electron. Lett.*, vol. 23, no. 3, pp. 109–110, 1987.

[6] M. J. W. Rodwell, C. J. Madden, B.T. Khuri-Yakub, D. M. Bloom, Y. C. Pao, N. S. Gabriel, and S. P. Swierkowski, "Generation of 7.8 ps electrical transcients on a monolitic transmission line," *Eletron. Lett.*, vol. 24, pp. 100–102, 1988.

[7] C. J. Madden, R. A. Marsland, M. J. W. Rodwell, and D. M. Bloom, "Hyperabrupt-doped gaas nonlinear transmission line for picosecond shock-wave generation," *Appl. Phys. Lett.*, vol. 54, pp. 1019–1021, 1989.

[8] M. J. W. Rodwell, M. Kamegawa, R. Yu, M. Case, E. Carman, and K. S. Giboney, "Gaas nonlinear transmission lines for picosecond pulse generation and millimeter-wave sampling," *IEEE Trans. Microwave Theory Tech.*, vol. 39, pp. 1194–1204, 1991.

[9] S. A. Maas, *Nonlinear Microwave Circuits*. Dedham, MA: Artech House, 1988.

[10] W. J. Rugh, *Nonlinear System Theory*. Baltimore, MD: The Johns Hopkins Univ. Press, 1981.

[11] R. Landauer, "Shock waves in nonlinear transmission lines and their effect on parametric amplification," *IBM J. Res. and Dev.*, vol. 4, pp. 391–401, 1960.

[12] R. H. Freeman and A. E. Karbowiak, "An investigation of nonlinear transmission lines and shock waves," *J. Phys. D*, vol. 10, pp. 633–643, 1977.

[13] D. Jäger and F.-J. Tegude, "Nonlinear wave propagation along periodic-loaded transmission line," *Appl. Phys.*, vol. 15, pp. 393–397, 1978.

[14] C. Camacho-Peñalosa and I. Molina-Fernandez, "Harmonic balance analysis of nonlinear transmission lines," *Electron. Lett.*, vol. 24, no. 19, pp. 1235–1236, 1988.

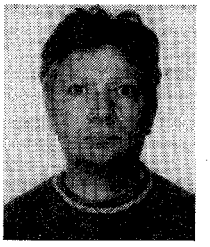

Patrick Celka (M'96) received the physicist degree from the Catholic University of Louvain-La-Neuve, Belgium in 1987, the master degree in signal and information processing from the Swiss Federal Institute of Technology, Lausanne, in 1991, and the Ph.D. degree in 1995 in nonlinear optical systems from the Chaire des Circuits et Systèmes, Swiss Federal Institute of Technology. His research area was from nonlinear electronic and optical circuits for telecommunications to chaotic systems and applications.

He is currently with the Signal Processing Laboratory, Swiss Federal Institute of Technology of Lausanne, where his research mainly concerns modelization of the cardiovascular system and, in particular, the relationships between the muscle sympathetic nerve activity and other classical cardiovascular signals.

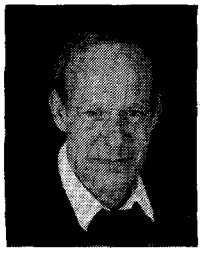

Martin J. Hasler (M'81–SM'90–F'93) received the Diploma in 1969 and the Ph.D. degree in 1973 from the Swiss Federal Institute of Technology, Zurich, both in physics. He continued research in mathematical physics at Bedford College, University of London, London, U.K., from 1973 to 1974.

At the end of 1974, he joined the Circuits and Systems group of the Swiss Federal Institute of Technology, Lausanne, where he became Professor in 1984. He was appointed Full Professor in 1996. During the 1970's, his research was concentrated on filter theory and design, in particular active and switched capacitor filters. In 1979, he started with nonlinear circuit theory, a new field for his institution. The main concern in the beginning was qualitative analysis of dynamic, and later also of resistive, circuits. In this context, he became interested in chaotic behavior of electric circuits. Later, he also became interested in artificial neural networks, as a special class of nonlinear circuits. Finally, he started research on modeling of nonlinear circuits and systems, as a complement to nonlinear circuit and system analysis. He collaborates with other researchers to bring the theory to bear on applications, in particular in the field of high-temperature superconductors with the power systems laboratory of the Swiss Federal Institute of Technology in Lausanne and with the University of Geneva, in the field of speech recognition with partners in Belgium and Germany (ESPRIT project of the EC) and in the context of neural networks within the MANTRA group of the Swiss Federal Institute of Technology in Lausanne. A new research project concerns the application of chaotic behavior in electrical engineering. He is the author and coauthor of about 100 research papers and four books, among them: *Nonlinear Circuits* (Boston, Artech House, 1986, co-authored by J. Neirynck) and *Recursive Neural Networks for Associative Memory* (London: Wiley, 1990, co-authored by Y. Kamp).

Dr. Hasler was the Editor of the IEEE TRANSACTIONS ON CIRCUITS AND SYSTEMS, PART I: FUNDAMENTAL THEORY AND APPLICATIONS from 1993 to 1995. He is also a member of the Editorial Board of *International Journal of Circuit Theory and Applications*, *Annales des Télécommunications and of Circuits, Systems and Signal Processing*. He is a member of the Swiss Physical Society, the European Circuits and Systems Society (ECS), and the European Society of Signal Processing (EURASIP).

Ataollah Azizi received the B.E.E. degree in 1976 from the Swiss Federal Institute of Technology, Lausanne, and the Ph.D. degree in 1982, also from the Swiss Federal Institute of Technology, mainly studying the behavior of microwave bipolar transistors under large-signal and nonlinear (class C) operation conditions.

After a period of practical work in the industry, he became a member of the Microwave, Electromagnetic, and Acoustics Group, Federal Institute of Technology. In 1982, he joined the Hasler Research Group, known now as Ascom Tech (Ascom Corporate Research), Bern, Switzerland, where he has been working in the field of broadband optical communications. His activities have mainly focused on the design and optimization of broadband low-noise optical front ends, design of high-speed OEIC's, studies of FITL, FTTC, and FFTH systems, analog CATV broadcast systems over fiber/coax, and the study and design of ATM over passive optical networks (PON's).